Understanding the role of oxygen-vacancy defects in $Cu_2O(111)$ from first-principle calculations

IOP Publishing Electron. Struct. 5 (2023) 035001 https://doi.org/10.1088/2516-1075/ace0aa

Electronic Structure

OPEN ACCESS

RECEIVED
10 March 2023

REVISED
27 April 2023

ACCEPTED FOR PUBLICATION
21 June 2023

PUBLISHED
4 July 2023

PAPER

Understanding the role of oxygen-vacancy defects in $Cu_2O(111)$ from first-principle calculations

Nanchen Dongfang[1], **Yasmine S Al-Hamdani**[2] **and Marcella Iannuzzi**[1,*]

[1] Department of Chemistry, University of Zurich, CH-8057 Zurich, Switzerland
[2] Department of Earth Sciences, University College London, London WC1E 6BT, United Kingdom
* Author to whom any correspondence should be addressed.

E-mail: marcella.iannuzzi@chem.uzh.ch

Keywords: Cu_2O, oxygen-vacancy defects, hybrid DFT

Supplementary material for this article is available online

Abstract

The presence of defects, such as copper and oxygen vacancies, in cuprous oxide films determines their characteristic carrier conductivity and consequently their application as semiconducting systems. There are still open questions on the induced electronic re-distribution, including the formation of polarons. Indeed, to accurately reproduce the structural and electronic properties at the cuprous oxide surface, very large slab models and theoretical approaches that go beyond the standard generalized gradient corrected density functional theory are needed. In this work we investigate oxygen vacancies formed in proximity of a reconstructed $Cu_2O(111)$ surface, where the outermost unsaturated copper atoms are removed, thus forming non-stoichiometric surface layers with copper vacancies. We address simultaneously surface and bulk properties by modelling a thick and symmetric slab, to find that hybrid exchange-correlation functionals are needed to describe the oxygen vacancy in this system. Our simulations show that the formation of oxygen vacancies is favoured in the sub-surface layer. Moreover, the oxygen vacancy leads to a splitting and left-shift of the shallow hole states in the gap, which are associated with the deficiency of copper at the surface. These findings suggest that surface electronic structure and reactivity are sensitive to the presence of oxygen vacancies, also when the latter are formed deeper within the film.

1. Introduction

Due to its availability, non-toxicity, and low cost, cuprous oxide (Cu_2O) is a well investigated semiconductor material. Thanks to its direct band gap of 2.17 eV [1], it finds applications for photovoltaic conversion in solar cells, photoelectron chemical water splitting [2, 3], and other catalytic processes. The high chemical activity of Cu_2O arises from the Cu^+ oxidation state, which can be either oxidised to Cu^{2+} or reduced to Cu^0, thereby facilitating a wide range of redox reactions. Further, Cu-based transparent conducting oxides are widely employed in nano-electronics and heterogenous catalysis [4].

The various applications are largely reliant on defects which are often responsible for the electronic performance. In particular, point defects tend to result in the emergence of localized states in the semiconductor band gap, and thereby play a key role on properties like the photoelectronic conductivity [5]. Both experiment [6] and theory [7–9] indicate that the defects play a central role in Cu_2O, however there is no general consensus on the underlying mechanisms on how they work. The experimental evidence suggests that the defect chemistry of Cu_2O is polaronic in nature [10], with contributions from copper vacancies (V_{Cu}), oxygen vacancies (V_O) as well as other ionic and electronic defects. In the bulk material, polarons lead to relatively deep hole trap levels [11], with Fermi level pinning in the band gap. This is responsible for the remarkably low open circuit voltages of 0.0–0.4 eV, resulting in poor performance when applied in solar cells [10]. On the other hand, research comparing a series of Cu_2O facets has found that $Cu_2O(111)$ presents higher catalytic activity and stability among the low-index facets of cuprous oxide, therefore, the

characterization of its surfaces and interfaces has attracted extensive interest both theoretically (*ab initio* methods) [12–14] and experimentally (XPS, LEED TEM) [15–17].

According to deep level transient spectroscopy, the acceptor levels caused by V_{Cu} are not localized, but rather form a band in the 0.45–0.55 eV range above the valence band maximum (VBM) [10, 18]. Density functional theory (DFT) calculations with the generalized gradient approximation (GGA) [8, 9, 19], instead, predict V_{Cu} delocalized hole states across the Fermi level, and a quasi-metallic character, rather than a polaronic conducting mechanism for p-type conductivity. The deficiencies of GGA-based methods in properly modelling the polaronic nature of p-type conductivity has been already recognized by Scanlon *et al* [10], who proposed to apply higher level of theories, such as hybrid functionals to achieve more reliable results. When using a screened hybrid-DFT (Heyd–Scuseria–Ernzerhof (HSE) hybrid functional [20]), distinct single particle levels associated with V_{Cu} defects appear within the band gap, consistent with experimentally known small polaron hopping mechanism. In addition, Isseroff and Carter [21] used DFT-HSE with more numerically stringent parameters and **k**-point sampling. In doing so, they demonstrated that DFT-HSE reproduces the correct electronic structure of the Cu_2O cation vacancies and the nature of the hole traps observed in experiments as well.

The presence of V_O in transition metal oxides has also an important influence on their semiconducting character. The charge density and atomic structure rearrangement around the vacant site affect the electronic conductivity, thus changing structural, electrical and optical properties as well as the photocatalytic performance [22]. Previous studies find that around each V_O site in Cu_2O the four equivalent copper atoms have unsaturated dangling bonds and act as a source of electron density, thus contributing to n-type character [23]. However, this interpretation has not reached a general consensus [8, 19, 24]. First-principles calculations have been performed to assess their role as electron-donating defects. Raebiger *et al* [19] apply DFT-GGA augmented with the Hubbard model (+U) and assert that the oxygen vacancies are unable to act as donors, because no ionization levels within the band gap has been revealed. They also estimate a low defect formation energy under Cu-rich/O-poor conditions, and conclude that V_O defects are stable only in the charge neutral state. Also based on GGA-DFT calculations, Soon *et al* [8] report that the presence of V_O introduces an occupied singlet state deep in the valence band and an empty triplet state inside the conduction band, thus resulting in a charge neutral defect, with no ability to compensate produced holes. On the other hand, the hybrid-DFT study of V_O defects by Scanlon and Watson [24] found no indication that the oxygen vacancies act as donors in Cu_2O, because no defect state is located in the band gap. Photoluminescence experiments, however, indicate n-type conductivity in Cu_2O, with oxygen vacancies acting as donors. Furthermore, a combined experimental and theoretical work by Nandy *et al* [25] based on GGA-DFT shows that oxygen vacancies can enhance the electron donating ability in Cu_2O, because of the unshared Cu-3d state which stretch toward the conduction band, forming an impurity energy (donor) state. They also discuss the work function dependence on the V_O concentration, which may lead to the Fermi level pinning, and consequent enhancing of the electron tunnelling proficiency of the surfaces. In summary, the available theoretical studies seem to suggest that un-doped n-type conductivity in Cu_2O is not driven by simple V_O defects, but the presence of V_O can increase the catalytic ability by decreasing the work function.

Given the sensitivity of predictions for Cu_2O to the level of theory applied from DFT and the unresolved questions that remain regarding vacancy defects at the surface, a thorough analysis of V_O and V_{Cu} in Cu_2O is desirable. Current experimental findings will be explained by an insightful knowledge of the function of V_O, which may be seen theoretically by considering how it operates in semiconductor devices or catalytic reactions situated on the surface or interface of Cu_2O. It is crucial for further advancements in abundant Cu_2O-based materials, particularly for the development of p–n heterojunctions for Cu_2O-based photovoltaic devices [24] and the adsorption and dissociation of gases (O_2 [26], NO [27], CS_2 [28] *etc*) On photocatalysis, Khasanah *et al* [29] pointed out that the dominating effect of V_O in Cu_2O remains to be determined, because it exerts opposite effects by facilitating the photocharge recombination and reducing the high reaction overpotential at the interface. Further, Kumar *et al* [30] demonstrate that due to the suitable band gap, Cu_2O are widely employed as the photocathode and the photoanode in photoelectrochemical water splitting, and enhance its productivity by tuning nanostructures, such as by introducing defects or dopants. In lithium-ion battery investigation, Cu_2O-based materials are commonly used as electrodes where V_O defects can improve the reaction kinetics by reducing the energy barrier of ion intercalation and accelerating the charge transfer [31]. Meanwhile V_Os are native defects in transition metal oxides and their presence has a critical effect on the physicochemical properties of the oxide. The study of defects in Cu_2O serves as a benchmark for research on other transition metal oxides and unleash their potential in more fields, with better understanding the effects of the presence and diffusion of V_Os [32].

In this work, we modelled a large Cu_2O slab consisting of 8 atomic layers and 736 atoms in the unit cell. This allowed us to model bulk-like and surface properties simultaneously. In order to address the contradictions and uncertainties in V_O defects, reliable descriptions of the electronic characteristics of the

defects are acquired and accomplished through hybrid DFT. A reconstructed $Cu_2O(111)$ surface was built by removing all the outermost copper atoms, and forming a non-stoichiometric surface with copper vacancies. We find that at hybrid functional level, the semiconducting features with acceptor levels in the gap are correctly reproduced. Moreover, the oxygen vacancy induces a splitting and left-shift of the in-gap states, which suggest that surface electronic structure and reactivity are sensitive to the presence of oxygen vacancies.

2. Computational details

All simulations were performed using the Quickstep module of the CP2K program package [33]. The Kohn–Sham DFT [34, 35] within the hybrid Gaussian and plane waves framework was applied for the electronic structure calculations, where the interactions with the atomic cores is described through Goedecker–Teter–Hutter (GTH) pseudopotentials [36] and the molecular orbitals of the valence electrons are expanded in Gaussian type orbitals. We used DZVP-MOLOPT-GTH primary basis sets and auxiliary uncontracted basis sets to accelerate the calculation of the electron repulsion integrals for hybrid functionals simulations [37]. For O atoms, cFIT3 auxiliary basis sets were used, and cFIT9 were used for Cu atoms. The plane waves cutoff has been set at 600 Ry. All calculations were periodic in three dimensions, only at Gamma point and spin-polarized (unrestricted Kohn–Sham). We used and compared three different flavours of exchange and correlation schemes: A standard GGA functional, Perdew-Burke-Ernzerhof (PBE) funcational [38], PBE+U [39, 40], and the hybrid functional HSE06 [20]. We used a $3 \times 3 \times 3$ supercell (162 atoms) with the lattice constant of 4.28 Å for bulk calculations. The $Cu_2O(111)$ model has been obtained stacking eight O–Cu–O trilayers, in a simulation cell with lateral dimension 24.15×24.15 Å^2, corresponding to 4×4 unit replicas.

For the optimization of geometries the long-range dispersion interactions D3 [41] was used. For the self-consistent field optimization we applied the orbital transformation method with conjugate gradient, converging the energy down to 5×10^{-7} Hartree. All proposed structures have been fully relaxed at the PBE+U+D3 functional level of theory, with the Broyden–Fletcher–Goldfarb–Shanno [42] scheme and a force threshold of 1×10^{-3} Hartree/Bohr. At each optimized geometry we refined the electronic structure by an additional calculation using the hybrid functional HSE06. More computational details are provided in the supplementary information (SI) section S.1. The reported illustrations of structures and electronic distributions have been produced with the visualization tools VESTA [43] and VMD [44–51].

3. Results and discussion

3.1. Cu_2O Bulk with V_{Cu}

A first assessment of the computational approach is provided by reproducing some properties of the bulk system, i.e. the electronic structure of pristine Cu_2O and the formation energy of one V_{Cu} as well as the induced electronic rearrangement. We obtain a bulk energy gap of 0.56 eV using PBE+U ($U = 2$ eV) and 1.74 eV using HSE06. The band gap of HSE06 is closer to the experimental value (2.17 eV) [1]. Removing one Cu atom from the bulk (figure 1(b)) and relaxing the structure at the PBE+U level, we observe some contraction of the Cu–O and Cu–Cu distances involving the first neighbours of the vacancy site, i.e. the Cu–O distance shortens to 1.84 Å from 1.86 Å, and the Cu–Cu distance shortens to 2.94 Å from 3.03 Å. The PBE+U projected density of states (PDOS), shown in the SI, is not significantly modified by the presence of the vacancy, since no defect states appear within the gap (figure S.5).

By computing the electronic structure of the optimized geometry at the HSE06 level of theory, one unoccupied (hole) spin down state appears within the energy gap, at 0.57 eV above the VBM (figure 1(b)). From the spatial distribution of this hole state (figure 1(c)), we observe that it is localized mainly on one Cu atom that was coordinated to the same O as the vacant Cu atom, and partially also on two Cu atoms in the vicinity of the defect site. It can be seen that the hole has a Cu_{3d} character with a small O_{2p} contribution. These results are in agreement with the previous hybrid functional calculations by Isseroff and Carter [21], who found a single particle state 0.46 eV above the VBM, and Scanlon *et al* [10], who also discuss a single-particle state 0.52 eV above VBM. The small numerical difference can be attributed to the use of different system size and calculation parameters.

By comparing the band gap values calculated at various theoretical levels—where the hybrid functional predicts a more acceptable band gap—and the electronic characteristics of the defective structure, we were able to demonstrate that HSE06 can produce plausible explanations for defects in related systems that are consistent with both experimental and other theoretical results [10, 18, 21].

3.2. $Cu_2O(111)$-V_{Cu}

A just-cleaved stoichiometric $Cu_2O(111)$ film is obtained as stacking of O–Cu–O trilayers, and could expose either oxygen or copper termination. The O-terminated surface consists of an outmost atomic layer of

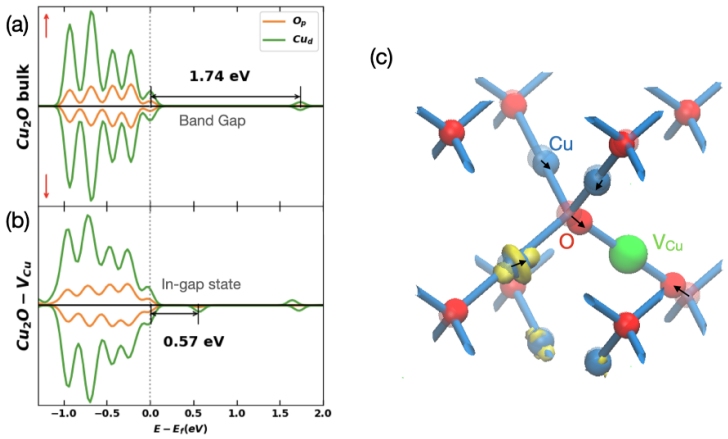

Figure 1. HSE06 projected DOS obtained from (a) bulk Cu_2O and (b) bulk Cu_2O with V_{Cu}. (c) Relaxed structure around the V_{Cu} (green sphere). The transparent spheres indicate the positions of the atoms before relaxation. The arrows highlight the displacement. The spatial distribution of the spin-down in-gap state is illustrated by the yellow isosurface, obtained at the density value of 0.03 el./Bohr^3.

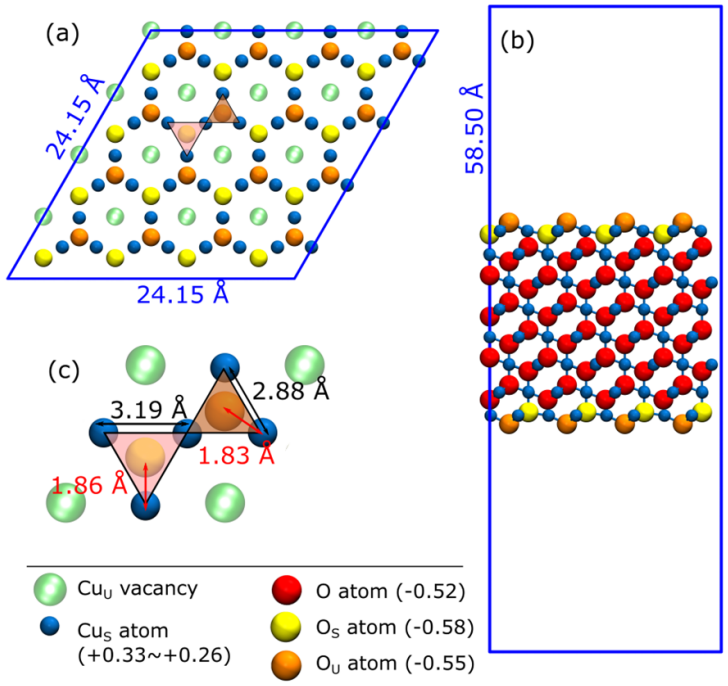

Figure 2. (a) Top layer of $Cu_2O(111)$-V_{Cu} after relaxation, where the position of the Cu_u vacancies is marked in green. (b) Side view of the $Cu_2O(111)$-V_{Cu} slab model. The blue profiles in) and (b) indicate the borders of the simulation cell. (c) The brown and red triangular shadowed areas highlight the coordination environment around O_u and O_s species, respectively. The numerical labels report the distances after relaxation. The colour code is reported at the bottom of the figure, where the values in brackets are the calculated HSE06 Mulliken charges.

unsaturated oxygen atoms (O_u), a second layer of copper, and a third layer of saturated oxygen atoms (O_s) atoms. The Cu atoms between the two oxygen layers can be classified into two groups, according to their bonding environment, i.e. saturated (Cu_s) and unsaturated (Cu_u) copper atoms. Previous studies [12, 23, 25, 52–54] have considered two possible models for the $Cu_2O(111)$ surface, the stoichiometric (non-polar) surface and the non-stoichiometric (polar) surface, where the Cu_u atoms are removed. Thermodynamic analysis shows that the Cu_u poor surface becomes increasingly more stable at higher oxygen chemical potential [53, 54]. In agreement with this, DFT predicts a lower surface energy for the reconstructed surface obtained by removing all Cu_u ions [16]. Hence, our simulations take as reference a model slab of eight trilayers, where from both surfaces all Cu_u atoms have been removed, thus introducing surface Cu vacancies. The lateral dimension is 24.15×24.15 Å^2, corresponding to a 4×4 super cell, where the bulk lattice constant is 4.28 Å, comparing to 4.27 Å in experiment [1]. The resulting structure is illustrated in figure 2 and we refer to it as $Cu_2O(111)$-V_{Cu}.

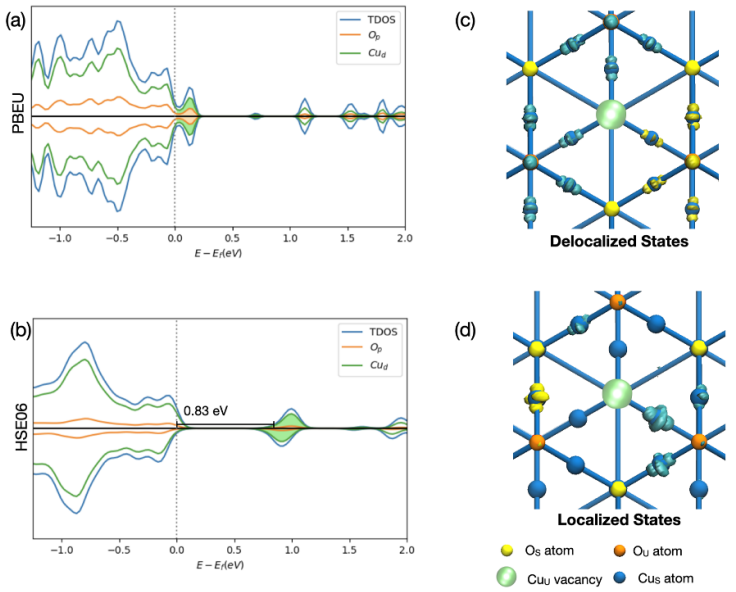

Figure 3. Left: Projected DOS obtained from the $Cu_2O(111)$-V_{Cu} slab at the at PBE+U (a) and HSE06 (b) level of theory. The features corresponding to the surface hole states are marked by shaded areas. Right: Spatial distribution of the in-gap surface hole states in the vicinity of one V_{Cu} calculated at PBE+U (c) and HSE06 (d) level of theory. The rendering is obtained using a density iso-value of 0.02 el./Bohr^3 (yellow spin-up cyan spin-down).

We take the $Cu_2O(111)$-V_{Cu} model as the reference structure. The resulting slab is no longer stoichiometric, owing to the vacant copper positions. Upon relaxation, both surface layers undergo some structural rearrangements, while the middle trilayers maintain the equilibrium bulk structure, which confirm that the slab thickness is appropriate to describe the surface properties. Panel (a) of figure 2 shows the top layer, where each oxygen atom is coordinated with three copper atoms, forming a pattern of interconnected triangles, where the oxygen atoms sit in the centre. Upon relaxation, the Cu–O and Cu–Cu distances around the unsaturated oxygen become slightly shorter with respect to equilibrium bulk (i.e. 1.83 vs 1.86 Å and 2.88 vs 3.03 Å, respectively). Correspondingly, the Cu–Cu distances around the saturated oxygen are slightly elongated (i.e. 3.19 Å). The structural changes are similar to those in Cu_2O bulk with a single V_{Cu}.

The structural relaxation at the surface is combined with the electronic rearrangement. As discussed in previous works [10, 11, 19, 21] and the last subsection, PBE and PBE+U methods fail in predicting the correct band structure and defect energy levels. It should be noted that the PBE exchange–correlation functional is a continuous extrapolation of the exchange-correlated energy of homogeneous electron gas, and in this approximation, self-interaction error (SIE) is inherent in PBE. As a result, the description for insulator and semiconductor systems exhibit flaws, and especially for highly correlated systems involving d- and f-electron, as Cu_2O, the band gaps and band structures are grossly underestimated. Therefore we refine the characterization of the electronic structure of the PBE+U optimized geometries by HSE06 single point energy calculations. In doing so, our work also confirms that different electronic properties are predicted with PBE+U and HSE06 levels of theory for the defective $Cu_2O(111)$ surfaces. Specifically, HSE06 predicts more localized states than PBE+U. The Mulliken population analysis shows that the Cu atoms at the surface become slightly more positive with respect to bulk (+0.32 vs +0.26 with our settings). Accordingly, the oxygen atoms within the surface trilayer acquire some additional negative charge (see figure 2). Figures 3(a) and (b) display the PDOS computed at the PBE+U and HSE06 levels of theory (see also SI figure S.6). In both cases we observe the appearance of one feature within the gap. These are the 16 acceptor states (empty) in each of the spin channel, corresponding to the 16 V_{Cu} at the surface. These electronic (hole) states are located at the surface and subsurface atoms and not in the bulk region of the slab, as shown by the spatial distributions depicted by isosurfaces in figures 3(c) and (d). PBE+U places the hole states just above the valence band, between the VBM and VBM+0.5 eV, such that the defect band crosses the Fermi level, resulting in a notionally metallic distribution. The spatial distribution (figure 3(c)) involves all Cu atoms around each V_{Cu} vacancy (six Cu on the surface, and three Cu on the subsurface). On the other hand, HSE06 predicts defect states with mainly Cu_{3d} character, and only small contributions from O_{2p} states. The spatial distribution also suggests major contributions on the surface and subsurface copper atoms, though, not all Cu atoms around V_{Cu} are involved. Only five out of nine neighbouring Cu atoms contribute to the defect state, in disagreement with PBE+U. Moreover, according to HSE06, the defect states are acceptor states in the

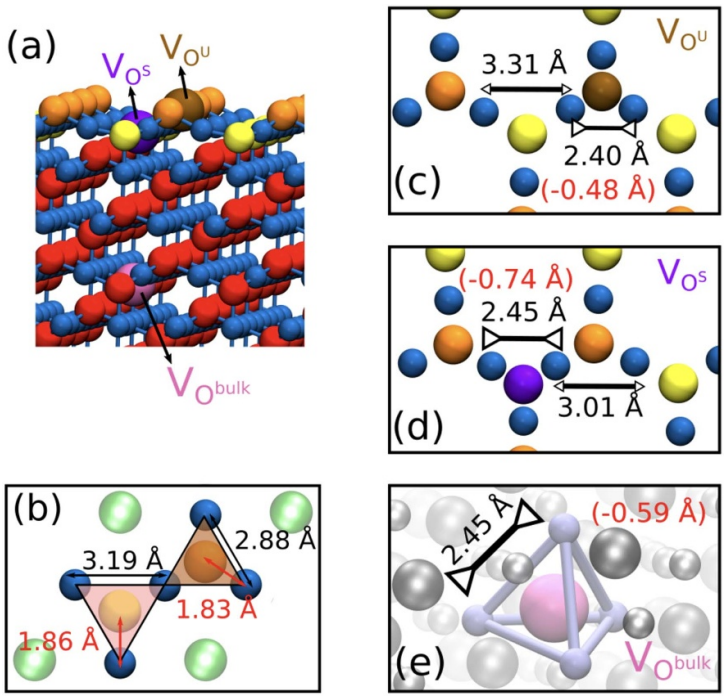

Figure 4. (a) Side view of $Cu_2O(111)$-V_{Cu}, where the spheres coloured in brown, violet and pink highlight the position of the three studied vacancy sites. (b) Top view of $Cu_2O(111)$-V_{Cu} surface layer. (c) V^u_O, (d) V^s_O, (e) V^b_O local atomic structures, after relaxation at PBE+U+D3 level. The Cu–Cu interatomic distances around the oxygen vacancy sites are reported in black with outward (inward) facing arrows indicating an increase (decrease) in distance. The Cu–Cu interatomic distances and distance variations with respect to the reference are also reported next to the arrows.

middle of the energy gap of the bulk, at about 0.8 eV from VBM. This is consistent with the experimental findings, revealing states in the range 0.12–0.70 eV above Fermi level, also associated to copper vacancies [10, 18, 55, 56]. These results assess the reliability of our model for the characterization of the $Cu_2O(111)$ surface and confirm that using the very large simulation cell and HSE06, we can correctly reproduce the properties of defective Cu_2O for both bulk and surface Cu vacancies.

3.3. Oxygen-vacancy defect

Single neutral oxygen vacancies have been introduced by removing one oxygen at three different sites: two of them within the surface trilayer, and one within the bulk region in the middle layer. Since placing one vacancy at the surface generates an asymmetric slab structure, which could lead to some artifact, we also considered the symmetric case, where two almost equivalent vacancies are placed at the two opposite surfaces. The neutral oxygen vacancy formation energy is evaluated as:

$$E = [(E_{\text{slab-O}} + N_{V_O} E_{O_2}/2) - E_{\text{slab}}]/N_{V_O} \quad (1)$$

where the $E_{\text{slab-O}}$ is the total energy of the defective slab, E_{O_2} is the energy of free-standing O_2 molecule, and E_{slab} is the energy of the $Cu_2O(111)$-V_{Cu} slab. N_{V_O} is the number of defects, i.e. one for the single V_O and two for the symmetric slab with two surface vacancies. As illustrated in figure 4, we use the following notation: V^u_O is the vacancy formed at the site of an unsaturated oxygen (surface layer), V^s_O refers to the vacancy within the surface sublayer, i.e. at the place of one O_s, and V^b_O is the vacancy in the bulk region.

3.3.1. Atomic structures

The structural rearrangements occurring upon full relaxation of the system with PBE+U+D3 are limited to the local region around the vacancy sites. In particular, the nearest neighbour Cu atoms that become unsaturated once the O atom is removed, move towards the vacant site (see figure 4 and SI). There are three Cu_{NN} atoms around V^u_O, while four Cu_{NN} atoms surround V^s_O as well as V^b_O. In all cases, the Cu_{NN}–Cu_{NN} distances shorten with respect to the reference structure, i.e. 2.40 vs 2.88 Å for V^u_O, 2.45 vs 3.19 Å for V^s_O, and 2.44 vs 3.03 Å for V^b_O. The Cu relaxation around V^u_O is less pronounced because of the reduced degrees of freedom of the topmost layer. The corresponding gain in energy along the geometry optimization after the oxygen atom has been removed, is significantly smaller, 2.9 eV, in comparison to the other two cases, e.g. 3.9 eV for V^s_O. The neighbours' shell around V^b_O turns out to undergo a contraction of the Cu–Cu distances,

Table 1. Oxygen vacancy formation energy in electronvolt, as computed by equation (1) at HSE06 level, on geometries fully relaxed at PBE+U+D3 level.

O vacancy site	V_O^u	V_O^s	V_O^b
One vacancy	2.74	2.47	2.73
Two vacancies	2.72	2.39	

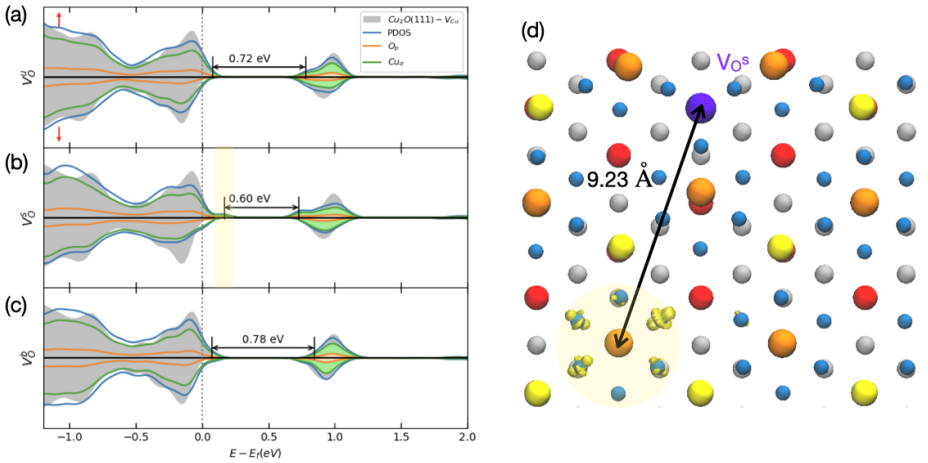

Figure 5. HSE06 projected DOS on the top trilayer in the presence of V_O. (a) V_O^u (b) V_O^s and (c) V_O^b. The grey shaded area corresponds to the reference PDOS (no V_O). All DOS are aligned by a common deep energy level, not affected by the defect. The zero is set at the Fermi level of the reference DOS. The value of band gap computed for the defective structures is reported in the respective panels. (d) Spatial distribution of the frontier state in (b) (shaded area). The rendering is obtained using a density iso-value of 0.02 el./Bohr^3. The arrow marks the distance between V_O^s and polaron's centre (9.23 Å).

while the Cu–O distances to the next neighbour oxygen atoms are elongated. This results in a four-membered Cu-cluster with unshared 3*d* states and partially reducing the electro-positivity of the cations according to Mulliken charges, which decrease by roughly 0.10 on each member of this Cu-cluster. Farther from the site of the vacancy no significant structural or charge rearrangement is observed.

3.3.2. V_O formation energy

table 1 lists the formation energies calculated for the three distinct V_O defects. The HSE06 energies are computed on the PBE+U+D3 optimized structure. V_O^u and V_O^b, turn out to be significantly less stable than the vacancy introduced in the sublayer. In the case of V_O^u this observation can be rationalized considering the much reduced relaxation around the vacancy site located at the very surface. In this region the structure is already strongly modified due to removal of the unsutured Cu atoms, therefore there is not enough flexibility to compensate for the missing oxygen. On the other hand, upon the formation of the vacancy within the bulk the energy drop along the relaxation is also large, 3.8 eV, due to the contraction of the first neighbour shell. However, there is a higher initial energy cost to removing an oxygen atom from the bulk-like region than from the subsurface and therefore, even after structural relaxation, the subsurface oxygen vacancy is the most thermodynamically favoured site.

We also testes the case of an symmetric model when the vacancy is created close to the surface, by placing a second vacancy on the opposite site of the slab at an almost equivalent site. The new structures have been relaxed with PBE+U+D3, and the electronic properties have been refined at the HSE06 level. The resulting geometric and electronic properties, as well as the formation energies turn out to differ only marginally from those obtained with the asymmetric slab.

3.3.3. Electronic structures

The HSE06 DOS projected onto the topmost trilayer of the $Cu_2O(111)$-V_{Cu} slab containing one of the described vacancy defects are reported in figure 5. We observe that the presence of V_O in the structure causes detectable modifications in the region of the VBM and in the in-gap states, associated to the surface Cu vacancies. The vacancy placed at the unsaturated oxygen site results in a slight shift in energy of the VBM and the in-gap states, probably owing to the reduced possibility of rearranging the electronic density among the neighbours. A larger effect is instead observed in the case of V_O^s, i.e. when the V_O is located at the sub-surface site, which results in a reduction of about 0.1 eV of the gap between the VBM and the in-gap states. In particular we observe that some additional Cu *d*-states get occupied at the VBM. The spatial distribution of

these states shows that they are localized on some Cu atoms of the sub-surface layer, just below an unsaturated oxygen site, as shown in figure 5. Hence, the excess negative charge resulting from the removal of one oxygen partially occupies the empty states resulting from the formation of the surface Cu vacancies, thus forming a polaron.

4. Conclusions

In this work we characterized Cu and O vacancies formed at $Cu_2O(111)$ by means of DFT calculations at the HSE06 level of theory applied to an unusually large slab model system. It has been confirmed that PBE and PBE+U give conflicting predictions for electronic properties of the defects even for this comparably large $Cu_2O(111)$ slab. Similar findings have been reported previously, showing that due to the SIE PBE fails to accurately characterize positive defects and predicts a semimetallic material instead of a semiconductor. HSE06, instead predicts localized in-gap defect states, which are associated to the removal of the unsaturated Cu atoms. The formation of one oxygen vacancy, both in the bulk or at the surface, induces a local relaxation around the defect corresponding to contraction of the Cu-atom coordination shell. No additional defect states are revealed within the gap. However, when the vacancy is placed in the sub-surface layer by removing a surface saturated oxygen, which is also the most favourable site for the formation of this defect, we could reveal the localization of a polaron. The polaron is displaced with respect to the vacant site, but still within the subsurface layer, and it has a Cu-d character. We conclude that HSE06 applied to the proposed slab model predict polaronic properties associated with the combined presence of V_O and V_{Cu} defects in Cu_2O. The results suggest that the neutral V_O defect induces the hole states splitting, which could enhance the electron mobility and boost the electronic activity at the surface, i.e. V_O in p-type Cu_2O (along with V_{Cu}) semiconductor can improve electron donating ability and its reactivity. In principle, the polaron can enhance conductivity as it can hop from Cu to Cu site, while exploiting the presence of the in-gap empty states and vibrational dynamics at finite temperature. More interestingly, it can potentially have an effect on the catalytic activity of the material. However, these are just speculation based on the behaviour of polarons in other oxides (see TiO_2 [57, 58]), since we have neither carried out simulations of the dynamics of the polaron nor on the effects on adsorbates. These could be topics of future work on this system.

Data availability statement

All data that support the findings of this study are included within the article (and any supplementary files). All calculation files will be available on the Materials Cloud (materialscloud.org) soon.

Acknowledgments

The authors are thankful for the generous allocation of computing resources from the Swiss National Supercomputing Center (CSCS) under Project ID s965, and both CSCS and the Alfred Werner-Legat for the computational resources under Project ID uzh35. N D thanks support from the NCCR MARVEL, a National Centre of Competence in Research, funded by the Swiss National Science Foundation (INSPIRE Potentials - MARVEL Master's Fellowship). Y S A thanks support from NCCR MARVEL and is supported by Leverhulme Grant No. RPG-2020-038.

ORCID iDs

Nanchen Dongfang https://orcid.org/0009-0000-9956-0101
Marcella Iannuzzi https://orcid.org/0000-0001-9717-2527

References

[1] Meyer B K *et al* 2012 Binary copper oxide semiconductors: from materials towards devices *Phys. Status Solidi* b **249** 1487–509
[2] Giordano L and Pacchioni G 2011 Oxide films at the nanoscale: new structures, new functions and new materials *Acc. Chem. Res.* **44** 1244–52
[3] Pan L, Kim J H, Mayer M T, Son M-K, Ummadisingu A, Lee J S, Hagfeldt A, Luo J and Grätzel M 2018 Boosting the performance of Cu_2O photocathodes for unassisted solar water splitting devices *Nat. Catal.* **1** 412–20
[4] Wu H, Zhang N, Wang H and Hong S 2013 Adsorption of CO_2 on Cu_2O (111) oxygen-vacancy surface: first-principles study *Chem. Phys. Lett.* **568–569** 84–89
[5] Borgwardt M *et al* 2019 Femtosecond time-resolved two-photon photoemission studies of ultrafast carrier relaxation in Cu_2O photoelectrodes *Nat. Commun.* **10** 2106
[6] Kitashima S, Kuroda A, Hirose K, Senna M, Yermakov A Y and Uimin M A 2007 Complex formation processes at the surface of Cu–O composite nanoparticles with and without external magnetic field *J. Alloys Compd.* **434–435** 646–9

[7] Soon A, Todorova M, Delley B and Stampfl C 2007 Thermodynamic stability and structure of copper oxide surfaces: a first-principles investigation *Phys. Rev.* B **75** 125420
[8] Soon A, Cui X-Y, Delley B, Wei S-H and Stampfl C 2009 Native defect-induced multifarious magnetism in nonstoichiometric cuprous oxide: first-principles study of bulk and surface properties of $Cu_{2-\delta}O$ *Phys. Rev.* B **79** 035205
[9] Nolan M and Elliott S D 2006 The p-type conduction mechanism in Cu_2O: a first principles study *Phys. Chem. Chem. Phys.* **8** 5350
[10] Scanlon D O, Morgan B J, Watson G W and Walsh A 2009 Acceptor levels in p-type Cu_2O: rationalizing theory and experiment *Phys. Rev. Lett.* **103** 096405
[11] Scanlon D O, Morgan B J and Watson G W 2009 Modeling the polaronic nature of p-type defects in Cu_2O: the failure of GGA and GGA+*U J. Chem. Phys.* **131** 124703
[12] Islam M M, Diawara B, Maurice V and Marcus P 2009 Bulk and surface properties of Cu_2O: a first-principles investigation *J. Mol. Struct.* **903** 41–48
[13] Nilius N, Fedderwitz H, Groß B, Noguera C and Goniakowski J 2016 Incorrect DFT-GGA predictions of the stability of non-stoichiometric/polar dielectric surfaces: the case of Cu_2O(111) *Phys. Chem. Chem. Phys.* **18** 6729–33
[14] Soon A, Söhnel T and Idriss H 2005 Plane-wave pseudopotential density functional theory periodic slab calculations of CO adsorption on Cu_2O(111) surface *Surf. Sci.* **579** 131–40
[15] Schulz K H and Cox D F 1991 Photoemission and low-energy-electron-diffraction study of clean and oxygen-dosed Cu_2O(111) and (100) surfaces *Phys. Rev.* B **43** 1610–21
[16] Zhang R, Li L, Frazer L, Chang K B, Poeppelmeier K R, Chan M K Y and Guest J R 2018 Atomistic determination of the surface structure of Cu_2O(111): experiment and theory *Phys. Chem. Chem. Phys.* **20** 27456–63
[17] Gattinoni C and Michaelides A 2015 Atomistic details of oxide surfaces and surface oxidation: the example of copper and its oxides *Surf. Sci. Rep.* **70** 424–47
[18] Noguet C, Tapiero M and Zielinger J P 1974 A new model for interpreting the electric conduction phenomena in Cu_2O single crystals *Phys. Status Solidi* a **24** 565–74
[19] Raebiger H, Lany S and Zunger A 2007 Origins of the p-type nature and cation deficiency in Cu_2O and related materials *Phys. Rev.* B **76** 045209
[20] Heyd J, Scuseria G E and Ernzerhof M 2003 Hybrid functionals based on a screened Coulomb potential *J. Chem. Phys.* **118** 8207–15
[21] Isseroff L Y and Carter E A 2013 Electronic structure of pure and doped cuprous oxide with copper vacancies: suppression of trap states *Chem. Mater.* **25** 253–65
[22] Singh M *et al* 2018 Oxygen-deficient photostable Cu_2O for enhanced visible light photocatalytic activity *Nanoscale* **10** 6039–50
[23] Frazer L, Chang K B, Schaller R D, Poeppelmeier K R and Ketterson J B 2017 Vacancy relaxation in cuprous oxide ($Cu_{2-x}O_{1-y}$) *J. Lumin.* **183** 281–90
[24] Scanlon D O and Watson G W 2010 Undoped n-type Cu_2O: fact or fiction *J. Phys. Chem. Lett.* **1** 2582–5
[25] Nandy S, Thapa R, Kumar M, Som T, Bundaleski N, Teodoro O M N D, Martins R and Fortunato E 2014 Efficient field emission from vertically aligned $Cu_2O_{1-\delta}$(111) nanostructure influenced by oxygen vacancy *Adv. Funct. Mater.* **25** 947–56
[26] Zhang R, Liu H, Zheng H, Ling L, Li Z and Wang B 2011 Adsorption and dissociation of O_2 on the Cu_2O(111) surface: thermochemistry, reaction barrier *Appl. Surf. Sci.* **257** 4787–94
[27] Sun B-Z, Chen W-K, Zheng J-D and Lu C-H 2008 Roles of oxygen vacancy in the adsorption properties of CO and NO on Cu_2O(111) surface: results of a first-principles study *Appl. Surf. Sci.* **255** 3141–8
[28] Chen H, Zhou S, Han Z, Jiang Y, Yu H, Zhou X, Jiang R, Liu X and Li X 2016 A copper-based sorbent with oxygen-vacancy defects from mechanochemical reduction for carbon disulfide absorption *J. Mater. Chem.* A **4** 17207–14
[29] Khasanah R A N, Lee C-H, Li Y C, Chen C-H, Lim T-S, Wang C-R, Chang P-Y, Sheu H-S and Chien F S-S 2022 Enhancement of photocatalytic activity of electrodeposited Cu_2O by reducing oxygen vacancy density *ACS Appl. Energy Mater.* **5** 15326–32
[30] Kumar S, Gupta B, A, Kumar R, Bharti A, Kumar A and Kumar V 2023 New insights into Cu/Cu_2O/CuO nanocomposite heterojunction facilitating photocatalytic generation of green fuel and detoxification of organic pollutants *J. Phys. Chem.* C **127** 7095–106
[31] Wang Y, Cao L, Huang J, Wang F, Kou L and Su Y 2023 Generation of Cu_2O hierarchical microspheres with oxygen vacancy on cu foam for fast Li-storage kinetics *J. Electroanal. Chem.* **930** 117149
[32] Lee S, Jin W, Kim S H, Joo S H, Nam G, Oh P, Kim Y-K, Kwak S K and Cho J 2019 Oxygen vacancy diffusion and condensation in lithium-ion battery cathode materials *Angew. Chem., Int. Ed.* **58** 10478–85
[33] Kühne T D *et al* 2020 CP2K: An electronic structure and molecular dynamics software package - quickstep: efficient and accurate electronic structure calculations *J. Chem. Phys.* **152** 194103
[34] Hohenberg P and Kohn W 1964 Inhomogeneous electron gas *Phys. Rev.* **136** B864–71
[35] Kohn W and Sham L J 1965 Self-consistent equations including exchange and correlation effects *Phys. Rev.* **140** A1133–8
[36] Goedecker S, Teter M and Hutter J 1996 Separable dual-space Gaussian pseudopotentials *Phys. Rev.* B **54** 1703–10
[37] Guidon M, Hutter J and VandeVondele J 2010 Auxiliary density matrix methods for Hartree-Fock exchange calculations *J. Chem. Theory Comput.* **6** 2348–64
[38] Perdew J P, Burke K and Ernzerhof M 1996 Generalized gradient approximation made simple *Phys. Rev. Lett.* **77** 3865–8
[39] Anisimov V I, Aryasetiawan F and Lichtenstein A I 1997 First-principles calculations of the electronic structure and spectra of strongly correlated systems: the ***LDA*** + *U* method *J. Phys.: Condens. Matter* **9** 767–808
[40] Himmetoglu B, Floris A, de Gironcoli S and Cococcioni M 2013 Hubbard-corrected DFT energy functionals: the LDA+U description of correlated systems *Int. J. Quantum Chem.* **114** 14–49
[41] Moellmann J and Grimme S 2014 DFT-D3 study of some molecular crystals *J. Phys. Chem.* C **118** 7615–21
[42] Head J D and Zerner M C 1985 A Broyden—Fletcher—Goldfarb—Shanno optimization procedure for molecular geometries *Chem. Phys. Lett.* **122** 264–70
[43] Momma K and Izumi F 2008 VESTA: a three-dimensional visualization system for electronic and structural analysis *J. Appl. Crystallogr.* **41** 653–8
[44] Humphrey W, Dalke A and Schulten K 1996 VMD – visual molecular dynamics *J. Mol. Graph.* **14** 33–38
[45] Stone J, Gullingsrud J, Grayson P and Schulten K 2001 A system for interactive molecular dynamics simulation *2001 ACM Symp. on Interactive 3D Graphics* ed J F Hughes and C H Séquin (ACM SIGGRAPH) pp 191–4
[46] Eargle J, Wright D and Luthey-Schulten Z 2006 Multiple alignment of protein structures and sequences for VMD *Bioinform.* **22** 504–6
[47] Stone J 1998 An efficient library for parallel ray tracing and animation *Master's Thesis* Computer Science Department University of Missouri-Rolla

[48] Frishman D and Argos P 1995 Knowledge-based secondary structure assignment *Proteins: Struct. Funct. Genet.* **23** 566–79
[49] Varshney A, Brooks F P and Wright W V 1994 Linearly scalable computation of smooth molecular surfaces *IEEE Comput. Graph. Appl.* **14** 19–25
[50] Sanner M, Olsen A and Spehner J-C 1995 Fast and robust computation of molecular surfaces *Proc. 11th ACM Symp. on Computational Geometry* (ACM) pp C6–C7
[51] Sharma R, Zeller M, Pavlovic V I, Huang T S, Lo Z, Chu S, Zhao Y, Phillips J C and Schulten K 2000 Speech/gesture interface to a visual-computing environment *IEEE Comput. Graph. Appl.* **20** 29–37
[52] Bendavid L I and Carter E A 2013 First-principles predictions of the structure, stability and photocatalytic potential of Cu_2O surfaces *J. Phys. Chem.* B **117** 15750–60
[53] Wu W, Zhao W, Wu Y, Zhou C, Li L, Liu Z, Dong J and Zhou K 2019 Antibacterial behaviors of Cu_2O particles with controllable morphologies in acrylic coatings *Appl. Surf. Sci.* **465** 279–87
[54] Hutchison M J and Scully J R 2018 Solute capture and doping of Al in Cu_2O: corrosion, tarnish resistance and cation release of high-purity Cu-Al alloys in artificial perspiration *J. Electrochem. Soc.* **165** C689–702
[55] Garuthara R and Siripala W 2006 Photoluminescence characterization of polycrystalline n-type Cu_2O films *J. Lumin.* **121** 173–8
[56] Paul G K, Nawa Y, Sato H, Sakurai T and Akimoto K 2006 Defects in Cu_2O studied by deep level transient spectroscopy *Appl. Phys. Lett.* **88** 141901
[57] Reticcioli M, Setvin M, Schmid M, Diebold U and Franchini C 2018 Formation and dynamics of small polarons on the rutile $Tio_2(110)$ surface *Phys. Rev.* B **98** 045306
[58] Reticcioli M, Sokolović I, Schmid M, Diebold U, Setvin M and Franchini C 2019 Interplay between adsorbates and polarons: CO on rutile $Tio_2(110)$ *Phys. Rev. Lett.* **122** 016805